Silicon nanowire-hydrogenated TiO2 core-shell arrays for stable electrochemical micro-capacitors

Yasmina Bencheikh, Ahmed Addad, Yannick Coffinier, Umesh Kumar, Pascal Roussel, Sabine Szunerits, Toufik Hadjersi, Mohammed Amin, Seddik El Hak Abaidia, Rabah Boukherroub

Version of Record: https://www.sciencedirect.com/science/article/pii/S0013468621014882
Manuscript_6d5b38330fb049f338912c09e19d84bc

Silicon nanowire-hydrogenated TiO_2 core-shell arrays for stable electrochemical micro-~~super~~capacitors

Yasmina Bencheikh[1,2,3], Ahmed Addad[4], Yannick Coffinier[1], Umesh Kumar[5], Pascal Roussel[6], Sabine Szunerits[1], Toufik Hadjersi[2], Mohammed A. Amin[7], Sidik El hak Abaidia[3], and Rabah Boukherroub[1*]

[1]*Univ. Lille, CNRS, Centrale Lille, Univ. Polytechnique Hauts-de-France, UMR 8520 - IEMN, F59000 Lille, France*

[2]*Research Center of Semiconductor Technology for Energy-2, Bd Frantz Fanon, BP 140, Alger 7 Merveilles 16038, Algiers, Algeria.*

[3]*Research laboratory: UR-MPE- Department of Physics, University of Boumerdes, Algeria*

[4]*Univ. Lille, CNRS, UMR 8207 – UMET, F-59000 Lille, France*

[5]*Univ. Lille, CNRS, Centrale Lille, Univ. Artois, UMR 8181 - UCCS, F59000 Lille, France*

[6]*CSIR-Indian Institute of Petroleum Dehradun-248005, India*

[7]*Department of chemistry, College of Science, Taif University, P.O. Box 11099, Taif 21944, Saudi Arabia*

*Correspondence author:

Rabah Boukherroub: rabah.boukherroub@univ-lille.fr

Abstract

In this paper, we fabricated silicon nanowire-TiO_2 core-shell arrays in a two-step process. First, silicon nanowire arrays (SiNW) were prepared in HF/$AgNO_3$ aqueous solution using metal-assisted chemical etching of bulk silicon. Then, atomic layer deposition (ALD) technique was applied to coat a 20 nm thin shell TiO_2 film. The TiO_2/SiNW substrates were afterward annealed at 400 °C in hydrogen atmosphere for 4 h and tested as electrode materials for electrochemical micro-~~super~~capacitors. The electrochemical features of the constructed H−TiO_2/SiNW electrode were assessed in an aqueous 1 M Na_2SO_4 electrolyte solution and revealed that the specific capacitance increased six times compared to non-annealed TiO_2/SiNW and 20-fold compared to a reference SiNW electrode under the same operating conditions. Importantly, H−TiO_2/SiNW also displayed a high stability over 30,000 cycles at 0.1 mA cm^{-2} with an overall decrease of 19% of the initial capacitance. The hydrogen treatment increased the density of hydroxyl group and enhanced the carrier density on TiO_2 surface improving the capacitive properties of H−TiO_2/SiNW.

Keywords: *Silicon nanowires; TiO_2 thin film; hydrogenation; micro-supercapacitor, high stability*

1. Introduction

Today, interest in energy saving, electric and hybrid vehicles and the quest for efficiency and multi-functionality in micro-systems make the research on electrochemical energy storage a field in full expansion [1, 2].

In particular, miniaturized versions of electrochemical ~~super~~capacitors (called micro-~~super~~capacitors) that can be easily integrated into microelectronic circuits attracted more attention in recent years [3-5]. Increasing the specific surface area and chemical stability of electrodes is the current research strategy to improve their performances in terms of storage capacity, life cycle, energy and power densities [6, 7]. In this case, it appears that nanostructured materials and in particular nanowires are the most suitable for the ~~super~~capacitor electrode realization, due to their high developed surface area and quasi-ideal electric double layer [8-11].

Silicon nanowires (SiNW) are one of these semiconductor nanostructures investigated as potential electrode material in energy storage/release devices like electrochemical ~~super~~capacitors [12] and batteries [13-15]. The focus on Si-based electrodes is essentially governed by the well-established microfabrication technology, which holds great promise in the area of integrated storage devices. In addition, large surface areas can be achieved through nanostructuration of bulk Si using different routes e.g. reactive ion etching (RIE), chemical vapor deposition growth, and metal-assisted chemical etching (MACE) [13, 15]. The latter approach, used in our work, is a simple and effective wet chemical approach to produce a nanowire array from bulk Si avoiding the use of vacuum environment.

Even though, SiNW arrays feature high developed surface area, their direct utilization as electrodes is restricted by their chemical instability in aqueous and basic solutions [9,11]. In fact, oxide formation and dissolution limit their long-term operation and real-world potential application. Therefore, coating of these nanowires with organic and non-organic materials

was commonly applied to overcome this hurdle. In this context, coating SiNW arrays with transition metal oxides (NiO, MnO_2, ZnO/Al_2O_3, and TiO_2) not only enhances the stability, but it also increases the specific capacity since they are battery-type or pseudo-capacitive materials [16-18]. Other coatings based on thin diamond [19, 20] and carbon [8, 21] films were also applied to enhance the capacitive performance of the SiNW electrodes.

TiO_2, one of these transition metal oxides, is the subject ~~to~~ of extensive academic and technological research, owing to its specific properties: non-toxic, abundant, inexpensive and chemically stable [22]. Despite its capacity is lower than that of other capacitive materials like RuO_2, NiO or conductive polymer nanostructures, it was broadly investigated as electrode material for electrochemical ~~super~~capacitors [23]. Investigation of the capacity of TiO_2 nanotubes revealed significantly high values (911 μF cm^{-1} at 1 mV s^{-1}) [24], and this value was improved upon hydrogenation treatment [25, 26]. Also, TiO2 as a transition metal oxide has been applied in perovskite devices [27, 28].

SiNW coated with TiO_2 (SiNW/TiO_2) were described in some reports. Konstantinou *et al.* used three processes to coat SiNW electrodes with TiO_2 thin film: $TiCl_4$ treatment ~~method~~, dip coating path and hydrothermal method [29]. The highest surface capacity (386 μF cm^{-2}) was achieved based on the galvanostatic charge-discharge (GCD) technique at 3.7×10^{-5} A in [Bmim][NTf_2] ionic liquid [29]. Besides, spin coating of TiO_2 on SiNW attained a specific capacity of 3.55 mF cm^{-2} at 0.1 mA cm^{-2} with a retention of 68.8% after 1,000 galvanostatic charge-discharge cycles [30].

Atomic layer deposition (ALD) is a technique able to afford compliant coatings on various substrates with a very precise control over the coating thickness [31]. Memarz *et al.* demonstrated that SiNW battery anode coated with TiO_2 by ALD featured a remarkable improvement in its performances, as compared to the non-coated one [32]. Although, TiO_2-coated electrodes achieved enhanced capacitive properties, their specific capacitance values

were significantly lower than those recorded using other metal oxides [24, 33, 34], most likely due to the limited electrochemical performance and reduced electrical conductivity of TiO_2 [35, 36].

One way to address these limitations is through hydrogenation, which is capable to modify effectively the material's properties. Indeed, it has been shown its great ability in TiO_2 nanocrystals for introducing significant structural changes and improvement in their optical, electronic, photocatalytic, lithium-ion storage capability and field emission [37].

Based on above results, we applied the ALD method to coat a thin TiO_2 layer on SiNW, prepared by Ag-assisted chemical etching, and subsequent thermal annealing at 400 ℃ for 4 h in hydrogen atmosphere. The effect of the H-TiO_2 coating on the capacitive behavior of the SiNW electrode was studied in 1M Na_2SO_4 aqueous electrolyte. The specific capacitance of H-TiO_2/SiNW was enhanced six times as compared to non-annealed one and 20-fold compared to a reference SiNW (4.5 µm) electrode under the same operating conditions. Furthermore, the hydrogenation of TiO_2 thin film deposited on SiNW led to good reversibility and stability over 30,000 galvanostatic charge-discharge cycles.

2. Experimental section

2.1.1. Preparation of TiO_2/SiNW

TiO_2 thin coatings were produced by ALD using $TiCl_4$ (titanium source), H_2O vapor (oxygen source), and nitrogen as the purge gas. The deposition was conducted at 260°C and 2.8 mbars using a pulse duration of 250 ms for both precursors separated by 2 s of N_2 purge. The thickness of TiO_2 is function of the number of cycles and was determined by ellipsometry on flat Si surface (placed alongside with SiNW substrates in the reaction chamber). We set all experimental ALD parameters to obtain TiO_2 thickness of 20 nm.

2.1.2. Hydrogenation process

The TiO_2/SiNW were subsequently annealed under hydrogen atmosphere (named here after as H-TiO_2/SiNW) and the other in the open air (designed as air-TiO_2/SiNW) both at 400 °C for 4 h. The hydrogenation time at the maximum temperature was 4 h per sample and the hydrogen flow was started 30 min before the thermal programming and continued until the sample attained room temperature. The total duration of the hydrogen flow was about 10 h.

3. Results and discussion

Figure S1 illustrates the scanning electron microscopy (SEM) micrographs of SiNW arrays produced by silicon dissolution in an aqueous solution of HF/$AgNO_3$ at 55°C for 30 min. The nanowires network forms bundles on the top surface due to inhomogeneous dissolution caused by Ag particles random distribution or van der Waals forces between the nanowires during the process of drying [38]. The cross-section observations revealed that a large quantity of nanowires well-aligned and perpendicular to the surface were obtained [39]. As it can be seen in **Figure S1b**, the wires are about 4.5 μm in length with different diameters. SEM images of a SiNW substrate ALD-coated with a TiO_2 thin film are depicted in **Figure 1. Fig. 1a** and **b** show that a thin film of TiO_2 was coated conformally on SiNW. The top view SEM images **(Fig. 1c,d)** confirmed that the TiO_2 layer was deposited in a uniform and conformal manner on the silicon nanowires. A TiO_2 film thickness of 20 nm was optimal to obtain high specific capacity and high cycling lifetime

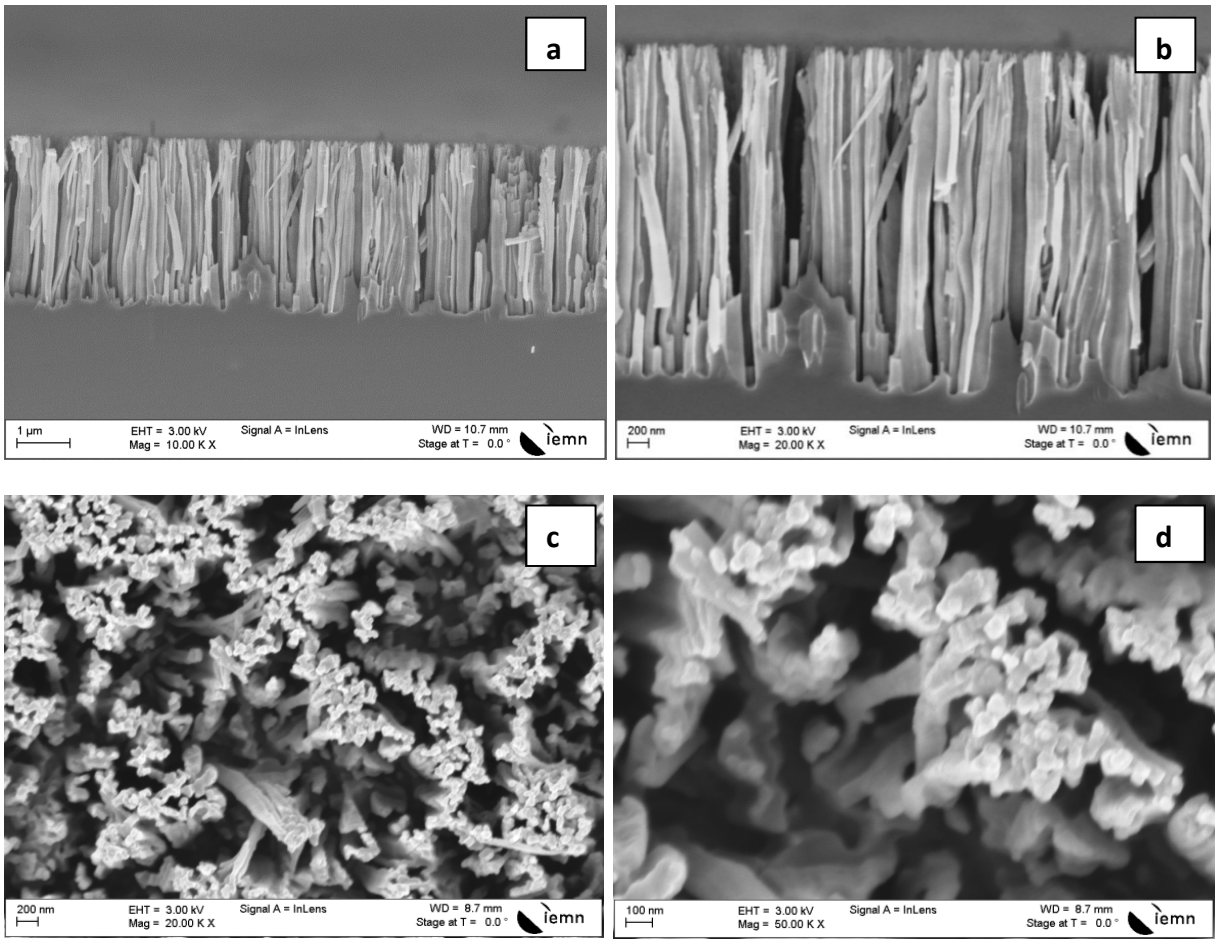

Figure 1: Cross-section (**a**,**b**) and top-view (**c,d**) SEM micrographs of SiNW arrays coated with 20 nm of TiO_2 by ALD.

To check if there is a change in the crystalline phase of TiO_2 after thermal hydrogenation, X-ray diffraction (XRD) patterns of TiO_2/SiNW and H-TiO_2/SiNW (400°C) were recorded. **Figure 2** displays the two diffractograms that present the same peaks at 2θ angles of 25.3°, 37.84°, 48.07°, 53.95° and 55.10° corresponding respectively to the (101), (044), (200), (105) and (211) diffraction planes. This indicates that the deposited TiO_2 phase is anatase (JCPDF No.21-1272) and that the thermal hydrogenation did not impact the TiO_2 crystalline structure [23, 40]. In addition to a slight decrease of the TiO_2 peak intensity after hydrogenation at high temperature, a small increase of the Full Width at ~~High~~ Half Maximum (FWHM) was observed, due most likely to increased defect density in TiO_2 structure, in accordance with

reference [40]. Note that the peak at 33° is due to the ~~lambda-half contamination of the (400)~~ (200) diffraction plan of the silicon substrate.

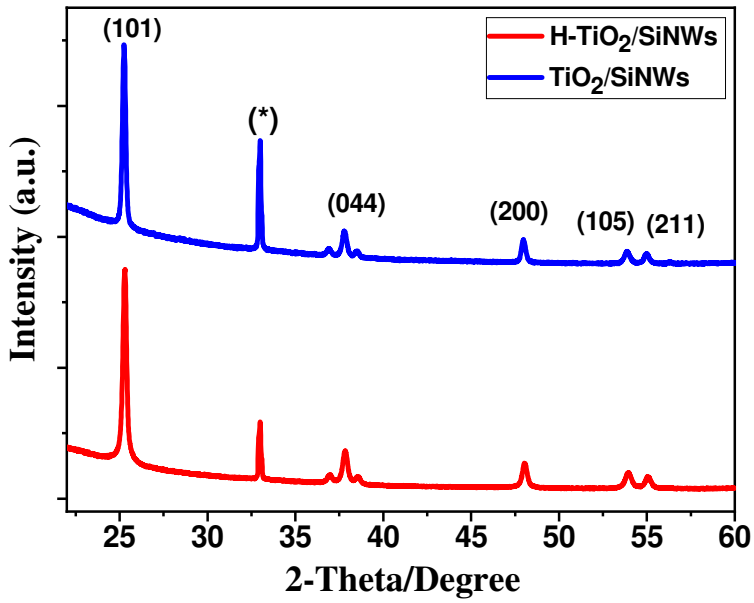

Figure 2. X-ray diffractograms of TiO_2/SiNW and H-TiO_2/SiNW samples.

To study in more detail the effect of the hydrogenation process on the phase structure, the TiO_2/SiNW and H-TiO_2/SiNW samples were characterized by Raman spectroscopy. The Raman plots are depicted in **Figure 3** and both comprise Raman bands at 397 cm^{-1} (B1g) and 640 cm^{-1} (Eg), characteristic of TiO_2 anatase. The width at mid-height of these two peaks were 36.05, 33.69 cm^{-1} and 33.47, 27.87 cm^{-1} respectively for the TiO_2/SiNW and H-TiO_2/SiNW samples. This means that the anatase phase is maintained after hydrogenation treatment, in accordance with XRD results. The Raman peaks of the H-TiO_2/SiNW sample are negatively offset and widen as compared to those of TiO_2/SiNW, which suggests an increase in the amount of vacant oxygen [41]. The feature at 520 cm^{-1} (*) is ascribed to the silicon substrate, its high intensity dominated the expected peak at 515 cm^{-1} (Eg), another characteristic peak of TiO_2 anatase which was not visible [42].

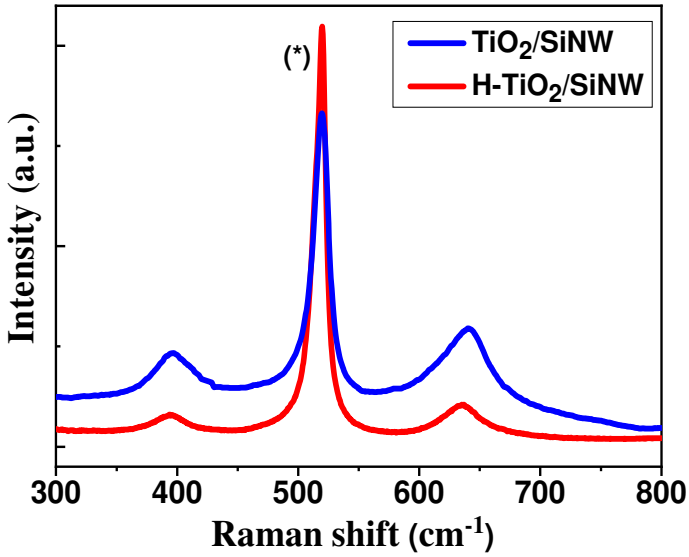

Figure 3. Raman plots of TiO_2/SiNW (blue) and H-TiO_2/SiNW (red) samples.

In order to determine surface chemical bonds, XPS data was acquired on the TiO_2/SiNW and H-TiO_2/SiNW substrates. The XPS survey profiles of TiO_2/SiNW and H-TiO_2/SiNW treated at 400 °C are comparable (see **Figure S2**). They both comprise Ti and O peaks characteristic of TiO_2 along with carbon signal originating from surface contamination during sample preparation and handling. The results infer that the hydrogenation process did not incorporate impurities into the TiO_2 lattice of H-TiO_2/SiNW.

Figure S3 displays the Ti_{2p} wide XPS scans of TiO_2/SiNW and H-TiO_2/SiNW. Both comprise peaks at 458.5 and 464.5 eV assigned respectively to $Ti_{2p3/2}$ and $Ti_{2p1/2}$, which are consistent with the typical values for TiO_2 [42-44]. **Figure 4a** and **b** depicts the O_{1s} plots of TiO_2/SiNW and H-TiO_2/SiNW. Both spectra can be deconvoluted with two bands at around 530 eV (Ti–O–Ti species) and 531 eV (–OH groups). The –OH peak intensity in the O_{1s} XPS spectrum increased after hydrogenation treatment, indicating the TiO_2 surface generated more surface hydroxyl groups [23]. The O peak remains the same meaning that the TiO_2 structure was not altered [45-47]. The result correlates well with the literature data [23], suggesting that hydrogen reacts with oxygen in TiO_2, resulting in defect formation in the system [47].

The valence band (VB) edge positions were determined to study the impact of the hydrogenation process on TiO_2 electron band structure. The VB positions of TiO_2/SiNW and H-TiO_2/SiNW were deduced from the XPS spectra (**Figure S4**). The comparison between **Figure S4a** and **b** reveals a blue-shift of the VB edge from 1.27 to 1.12 eV after hydrogenation treatment in accordance with the literature [40, 44, 45, 47]; this could be related to hydrogen reaction with oxygen on TiO_2 surface in accordance with XPS results quoted above.

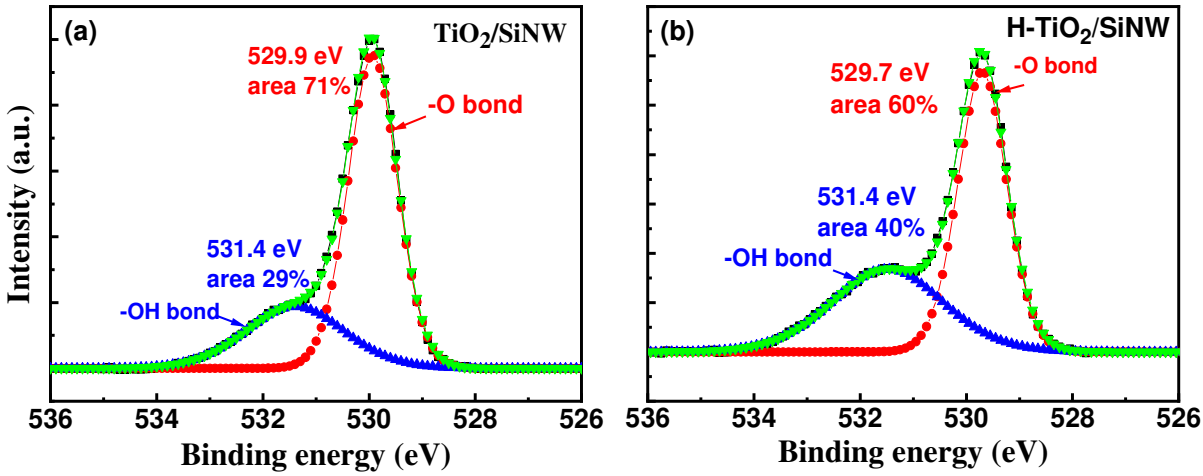

Figure 4. O_{1s} XPS high-resolution profiles of (**a**) TiO_2/SiNW and (**b**) H-TiO_2/SiNW surfaces.

Optical band gap was also estimated by using the Kubelka-Munk [K-M or F(R)] method (&**SI** for details). The determined values from diffuse reflectance spectra revealed that the band gap was blue shifted from 3.03 eV to 2.82 eV when TiO_2/SiNW sample was hydrogenated (**Figure S5**). A comparable shift was found after hydrogenation of TiO_2 [40, 44-47] and was assigned to the formation of more hydroxyl groups on the H-TiO_2 surface.

The structure of H-TiO_2/SiNW was studied by transmission electron microscopy (TEM), **Figure 5a**. An individual silicon nanowire uniformly coated by TiO_2 thin film with a diameter of about 130 nm could be evidenced. In **Figure 5c** is exhibited a zoom of selected area of the

image **b**, where a spacing of 3.5 Å between adjacent planes, assigned to anatase TiO_2 (101), is clearly visible. This value correlates well with the expected TiO_2 interlayer distance [39]. In addition, a thin amorphous layer near the crystalline surface is also evident, which is in accordance with previous reports on hydrogenated TiO_2 [37, 48].

We can see also, in supplementary information (**Figure S6**), a chemical analysis of the image area of 20 nm TiO_2 layer, the concentration is very close to TiO_2 (27% Ti – 70% O).

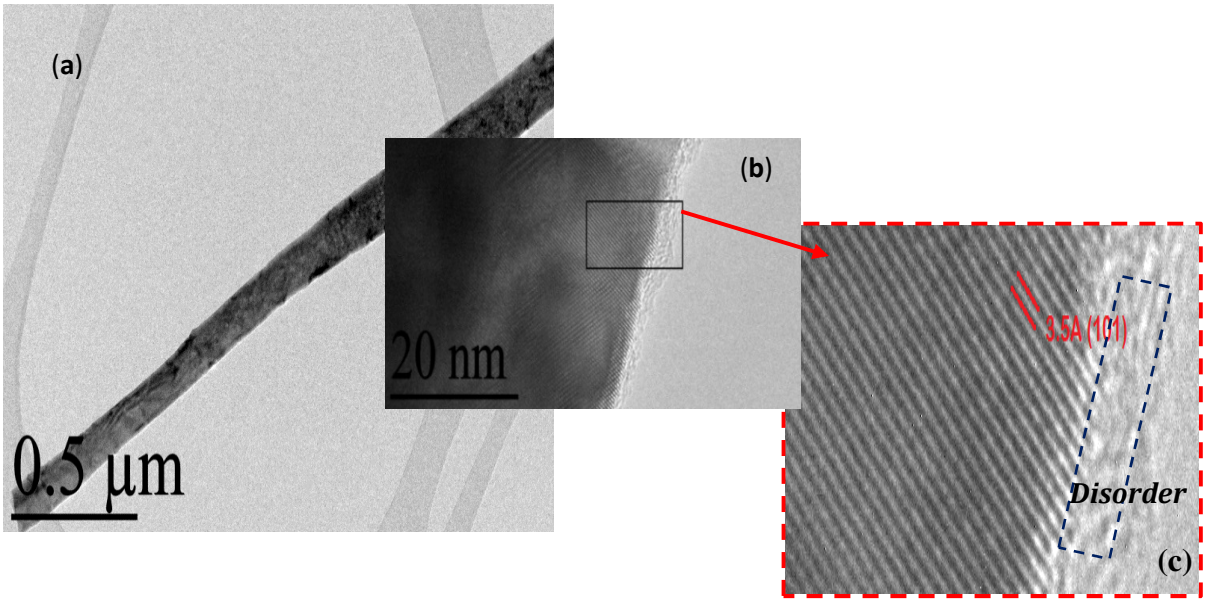

Figure 5. (**a**) Scanning transmission electron microscopy (STEM) of an individual H-TiO_2/SiNW; HR-TEM micrographs at low **(b)** and high **(c)** resolution. The thickness of TiO_2 is 20 nm.

Figure 6 depicts a STEM and the corresponding electron energy loss spectroscopy (EELS) plots recorded from the surface of hydrogenated TiO_2/SiNW; obvious changes in shape and position, shifting to lower energies, were observed as compared to the EELS acquired in the bulk TiO_2 in **Figure 6c**. This indicates that the surface shell around TiO_2 comprises hydroxyl species ascribed to diffusion of H atoms into the anatase TiO_2 [49]; this was not evidenced on the non-hydrogenated TiO_2/SiNW surface in **Figure 7** where the EELS spectra state the same in the shell (**Figure 7b**) and bulk (**Figure 7c**).

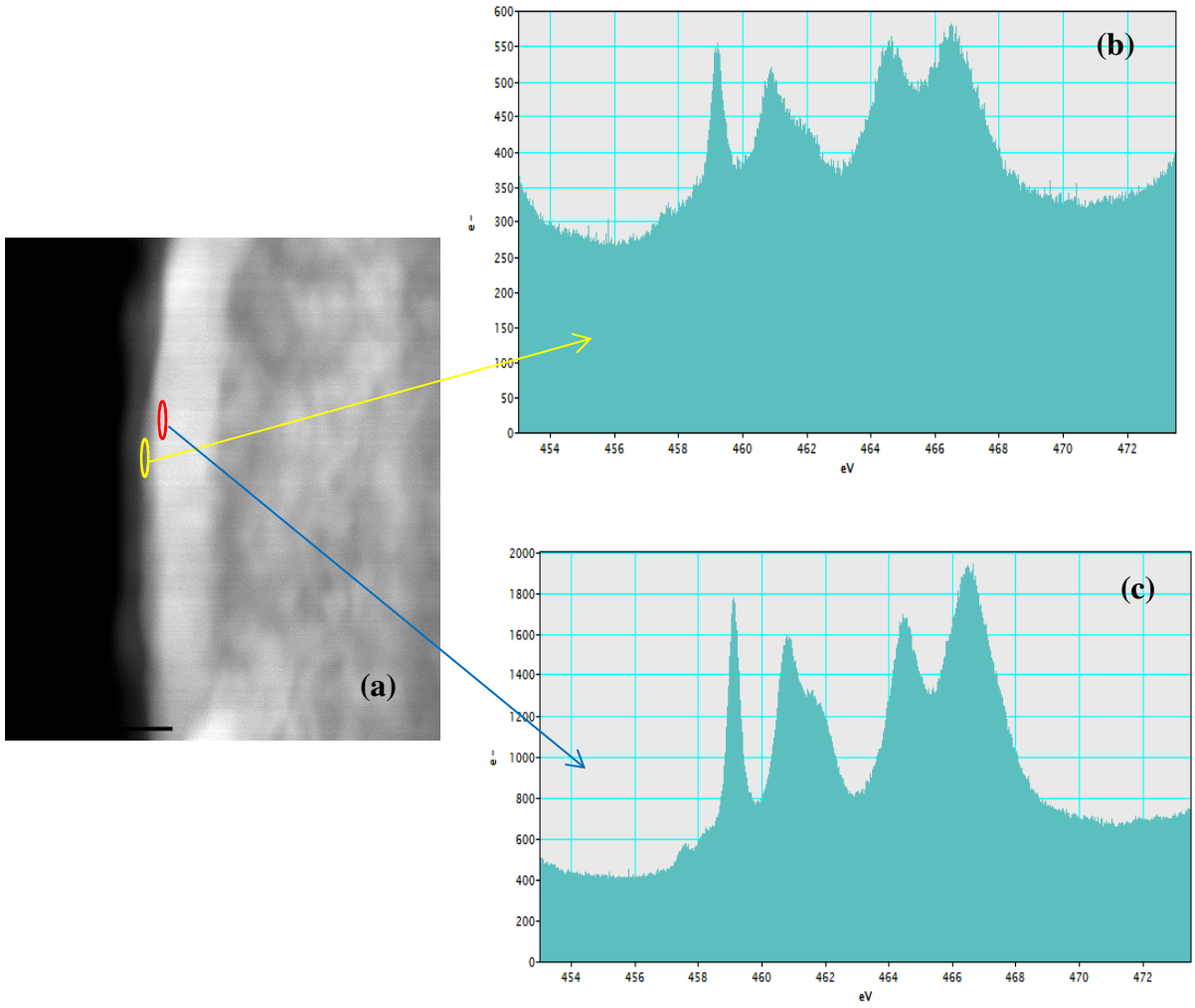

Figure 6. (**a**) STEM-HAADF image of TiO_2/SiNW surface; EELS spectra of (**b**) the extreme surface (less than 3 nm) and (**c**) 15 nm below the surface of TiO_2.

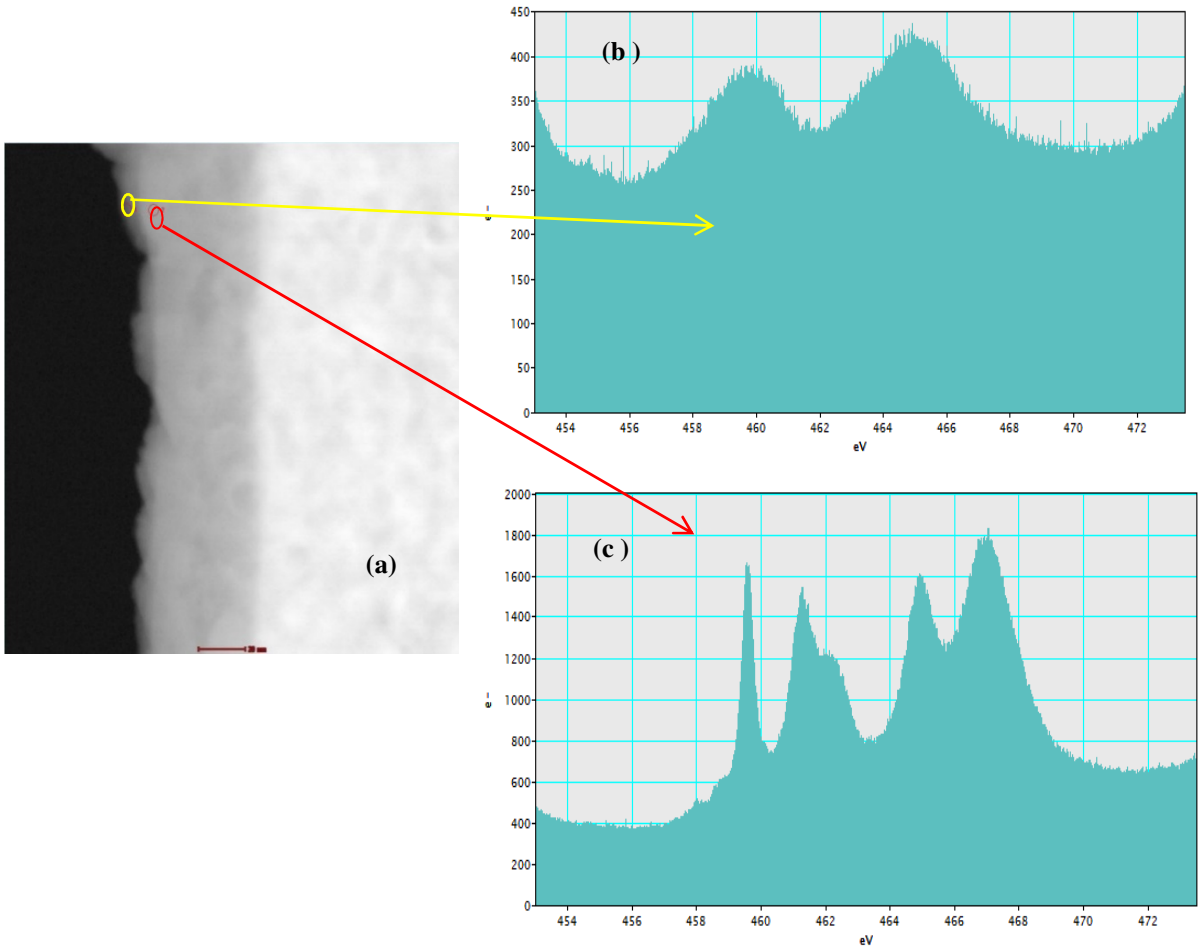

Figure 7. (**a**) STEM-HAADF image of H-TiO_2/SiNW surface; EELS spectra of (**a**) extreme surface (less than 3 nm) ~~Ti reduced~~ and (**c**) 15 nm below the surface of TiO_2.

The fabricated electrodes are characterized in a 3-electrodes electrochemical cell by cyclic voltammetry (CV), galvanostatic charge-discharge (GCD) and electrochemical impedance spectroscopy (EIS) in aqueous 1 M Na_2SO_4 solution using Ag/AgCl reference and platinum counter electrodes. **Figure 8a** displays the CV profiles of the uncoated SiNW, TiO_2/SiNW, air-TiO_2/SiNW and H–TiO_2/SiNW electrodes acquired at 100 mV s^{-1}. The plots feature a quasi-rectangular typical shape ascribed to the formation of an electric double layer at the electrode-electrolyte interface without any obvious redox peaks. It is obvious that H-TiO_2/SiNW attained largest current than SiNW, TiO_2/SiNW and air-TiO_2/SiNW electrodes [21].

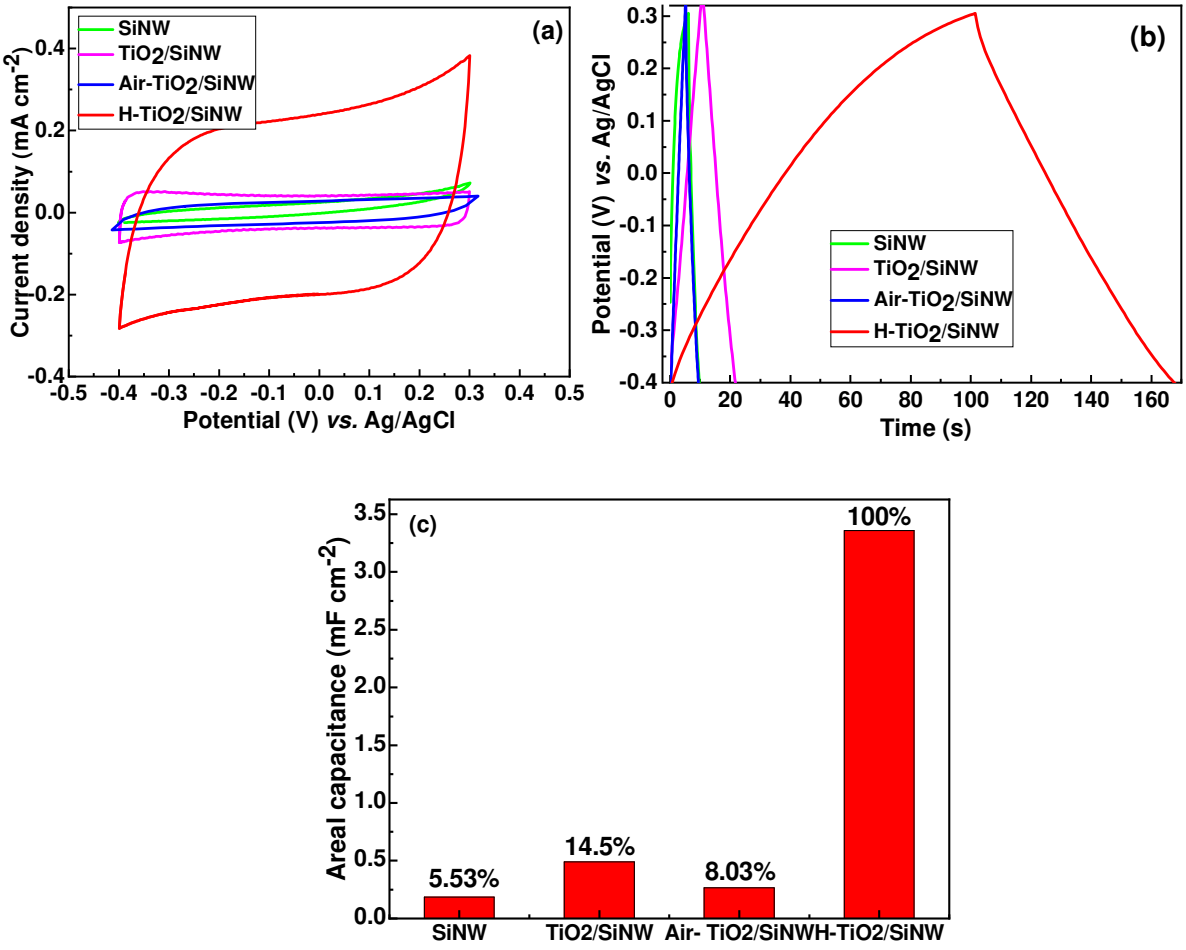

Figure 8. **(a)** CV plots of different electrodes collected at 100 mV s^{-1} in a potential range from -0.4 to +0.3V, **(b)** GCD profiles recorded at 0.035 mA cm^{-2}, (**c**) Areal capacitance of different electrodes acquired at 100 mV s^{-1}.

The specific capacitance was determined from the CV plots using equation (1):

$$C = \frac{\int j dV}{2 \times V \times r} \qquad (1)$$

C is the areal capacitance, j denotes the current density, V corresponds to the potential window, r represents the scan rate.

Additionally, the specific capacitance of the samples was determined from the GCD plots using equation (2):

$$C = j\frac{dt}{dV} \qquad (2)$$

dt denotes the time of discharge, *dV* represents the potential range, j corresponds to the current density.

The specific capacitance values are given in **Table 1.** The SiNW, TiO_2/SiNW and air-TiO_2/SiNW electrodes achieved specific capacities of 0.186, 0.489 and 0.265 mF cm^{-2}, respectively at 0.035 mA cm^{-2}. These values are comparatively smaller than that recorded for H-TiO_2/SiNW electrodes (3.36 mF cm^{-2}) under otherwise identical experimental conditions. The effect of annealing under hydrogen atmosphere is highlighted by the 6-fold enhancement of the capacitance value, in comparison to that of the sample annealed in air at the same temperature i.e. air-TiO_2/SiNW electrode. This improvement in energy storage capacity could be ascribed to improved conductivity, increased hydroxyl groups on the TiO_2 surface, and/or generation of oxygen vacancies. Comparable results have been reported by several research groups for TiO_2 nanotubes thermally annealed under hydrogen atmosphere [23], thermally annealed in air followed by chemical reduction using $NaBH_4$ [50], or through electrochemical hydrogen doping by water electrolysis [51].

Table 1: Areal capacitance of the prepared working electrodes in 1 M Na_2SO_4 deduced from the CV and GCD measurements.

Working electrode	**Technique used to calculate Areal capacitance ($mFcm^{-2}$)**	
	CV Scan rate=100 mVs^{-1}	GCD *J*= 0.035 mA cm^{-2}
SiNW	0.137	0.186
TiO_2/SiNW	0.434	0.489
Air-TiO_2/SiNW	0.227	0.265
H-TiO_2/SiNW	2.76	3.36

This areal capacitance is much larger than the literature data recorded for rGO-SiNW (240 μF cm^{-2} at 0.01 mA cm^{-2}) [52], HNO_3-oxidized *p*-type SiNWs (404 μF cm^{-2} at 50 mV s^{-1}) [53] and the best areal capacitance of 386 μF cm^{-2} recorded for TiO_2-coated SiNW array electrode in [Bmim][NTF2] at 3.7×10^{-5} A [29]. Our result is also better than that recorded for carbon-coated SiNW electrode (105 μF cm^{-2} at 1 V s^{-1} using cyclic voltammetry) [54], Si-NR/TiN electrode (1.08 mF cm^{-2} at 100 mV cm^{-2}) [55], and diamond-coated SiNW (1.55 mF cm^{-2}) using a cell voltage of 4 V [20]. The value is comparable to that reported for TiO_2-coated SiNW using spin coating [30]. A comparison table between the works already performed on TiO_2 electrode is given in the **supplementary information**.

The CV profiles of H–TiO_2/SiNW electrodes acquired at various scan rates showed nearly rectangular shape (**Figure 9a**). The improved capacitive behavior and high-rate capability of H–TiO_2/SiNW electrodes were proved by the unchanged shape upon changing the scan rate from 20 to 500 mV s^{-1}. The GCD plots of H-TiO_2/SiNW electrodes are depicted in **Figure 9b**. All curves displayed an almost ideal triangular shape, suggesting a good capacitive behavior in full accordance with the CV measurements. The areal capacitance values of untreated SiNW, TiO_2/SiNW, air-TiO_2/SiNW and H-TiO_2/SiNW electrodes recorded at different scan rates and current densities are compared respectively in **Figure 9c** and **d**. Upon increasing the scan rate and current density, a decline in the capacitance was evident; this behavior might be ascribed to restricted accessibility of parts of the surface to the electrolyte at high scan and charging-discharging rates. In fact, electrolyte ions diffusion into the electrode internal structure and pores is hindered at high scan rate and the interaction between the electrode surface and electrolyte becomes ineffective, thereby, the specific capacitance declines. This contrasts with low scan rates, where ions have sufficient time to diffuse deeply into pores, leading to enhanced specific capacitance. In addition, it is evident that the H-TiO_2/SiNW

electrode features the highest capacitance followed by TiO_2/SiNW and air-TiO_2/SiNW; such a behavior can be related to the enhancement of TiO_2 electrical conductivity upon hydrogenation [19]. The calculated areal capacitance of H–TiO_2/SiNW at a high scan rate (500 mV s^{-1}) was 1.56 mF cm^{-2}, which correlates with a capacitance retention of almost 61% as compared to the value recorded at 20 mV s^{-1}. The power loss was most likely due to reduced electrical conductivity (0.009–0.01 Ω cm) of the doped silicon substrate particularly at high scan rate [19].

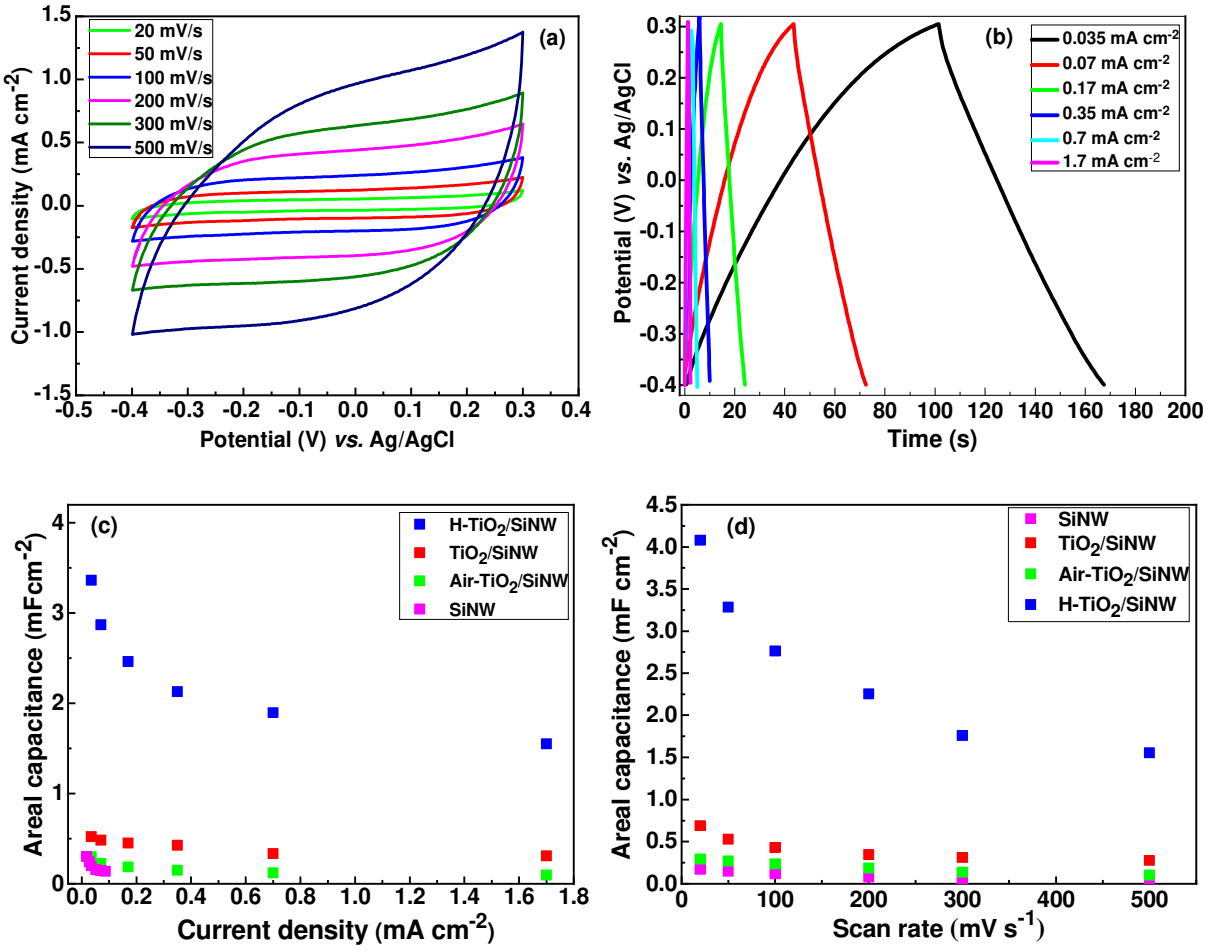

Figure 9. (**a**) CV plots of H–TiO_2/SiNW acquired at different scan rates (potential range: -0.4 to +0.3 V), (**b**) GCD plots recorded for H–TiO_2/SiNW at different current densities, (**c**) Areal capacitance of all electrodes *versus* scan rate, (**d**) Areal capacitance of all electrodes *versus* current density.

EIS was applied to examine the electrode/electrolyte interface and gain a better understanding on the electrochemical behavior and electrode kinetics. **Figure 10** depicts the Nyquist curves of H–TiO_2/SiNW and TiO_2/SiNW electrodes in 1M Na_2SO_4 within 100 mHz – 100 kHz frequency range at open circuit potential. The inset corresponds to the enlarged high frequency region for H-TiO_2/SiNW electrode. The plot comprises two main features: a single semicircular arc in the high frequency domain (inset) and a straight line in the low frequency region. The diameter of the semicircular in the middle section of Z' axis corresponds to the charge transfer resistance (R_{ct}) of the electrode. Moreover, the straight line (low frequency domain) infers that the charge storage capability of H–TiO_2/SiNW electrode is governed by rapid ion diffusion pathway. In addition, EIS analysis allowed to assess the evolution of the resistance before and after hydrogenation; the equivalent circuit is depicted in the inset of **Figure 10** (R_{ct}, R_s, C_{dl},W_o, and C_l are the charge-transfer resistance, internal resistance, double-layer capacitance, Warburg element, and limit capacitance, respectively). The R_s and R_{ct} values are dramatically reduced from initial 12.21 and 625.82 **Ω** to 10.47 and 90.13 **Ω** after hydrogenation, respectively, owing to improved electrical conductivity along with decreased ion diffusion resistance, as evidenced by the steeper line at low frequencies. Nyquist curves of TiO_2 and H-TiO_2 nanotube electrodes in [56] present the same decreasing trend after hydrogenation. Also, in our results, the high value of R_{ct} for the non-hydrogenated TiO_2/SiNW suggests a poor electrical conductivity of TiO_2 deposited thin film.

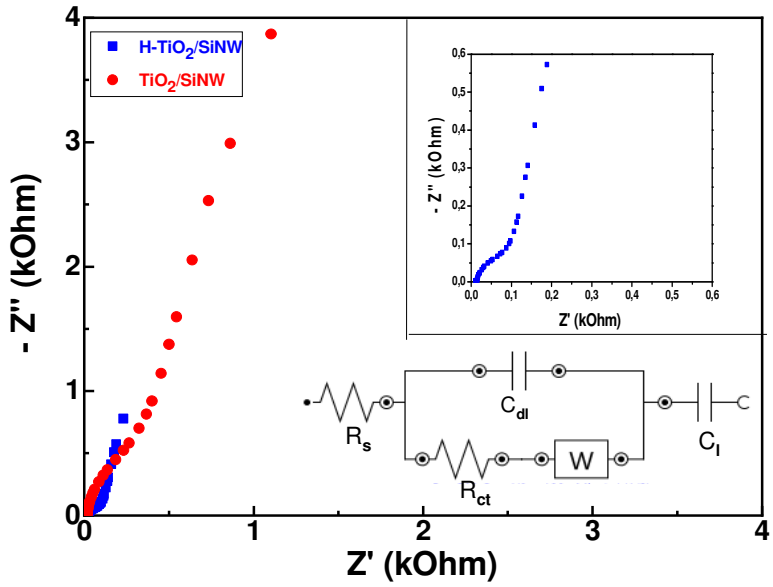

Figure 10. Nyquist plot in the 0.1 Hz to 5×10^5 Hz frequency range. Inset displays the enlarged region at high frequency for H-TiO_2/SiNW electrode.

Furthermore, EIS was also commonly applied to assess the capacitive behavior of electrochemical micro-~~super~~capacitors. Using equation (3), the imaginary part of the complex capacitance versus frequency can be determined [10]:

$$C''(\omega) = \frac{Z'(\omega)}{\omega|Z(\omega)|^2} \qquad (3)$$

where C″(ω) denotes the imaginary part of the capacitance, Z' (ω) corresponds to the real part of the impedance, Z(ω) is the impedance and ω=2πf (f is the frequency).

Figure S7 exhibits the plot of C″ *versus* frequency for the H-TiO_2/SiNW electrode. In addition, the relaxation time constant (τ_0), defined as the minimum time necessary to discharge all the energy from a supercapacitor with at least 50% efficiency, can be derived from this spectrum [10]. From the curve in **Figure S7**, a time constant of 2.05 ms was determined using the relation ($\tau_0=1/f_0$). The rapid frequency response of 0.5 Hz was ascribed to the porous architecture of the electrode, which provides full access to the electrolyte ions,

allowing a faster rate of diffusion. This value is lower than that reported for electrochemical micro-~~super~~capacitors based on SiNW electrodes (e.g. values 3.51 ms) [10].

High-performance electrochemical ~~super~~capacitors are commonly characterized by enhanced cycling stability. The H-TiO_2/SiNW stability was assessed by GCD for 30,000 cycles. The percentage of capacitance retention *versus* cycle number is exhibited in **Figure 11**. The electrode retained ~81% of its original specific capacitance after complete 30,000 cycles at 0.1 mA cm^{-2} in the -0.4 to +0.3 V potential window in 1 M Na_2SO_4. The result proved the good stability of the electrode after 30,000 cycles.

SEM imaging of the H-TiO_2/SiNW after the stability test revealed a similar morphology, testifying the high stability of the electrode material under our experimental conditions (data not shown). Also, this could be a good indication that the storage is mainly by EDL mechanism since in this case during the charging/discharging cycles, there is not an alteration of the structure of the electrode at the interface.

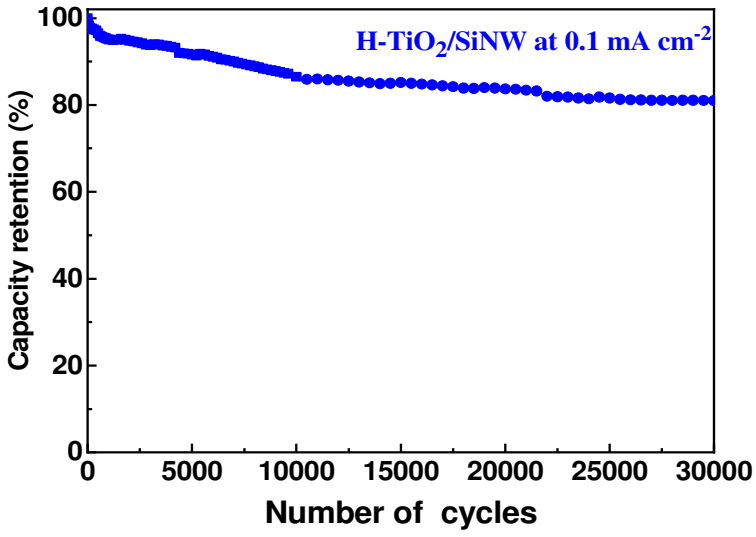

Figure 11. Life time testing of the H-TiO_2/SiNW electrode in an aqueous 1M Na_2SO_4 electrolyte**.**

Symmetric electrochemical ~~super~~capacitor devices

Using a classical 2-electrode symmetric configuration cell (**Figure S8**), we tested our electrode for its potential application in energy storage devices [57]. Both the cathode and anode consisted of H-TiO_2/SiNW core-shell electrodes and 1 M Na_2SO_4 aqueous electrolyte. Interestingly, the device exhibited nearly rectangular CV plots (**Figure 12a**) and symmetrical triangular GCD profiles (**Figure 12b**), indicating the good capacitive performance. Upon increasing the scan rate from 0.02 to 0.1 mV s^{-1}, the cell capacitance remained at 76.5% (decrease from 2.89 to 2.14 mF cm^{-2}), **Figure 12c**. The specific capacitance was determined from the CV plots using Eq.1 multiplied by a factor 2 (the factor 2 is due to the two symmetric electrodes construction) [58]. In the same configuration, as in the case of CV measurements using 1 M Na_2SO_4, GCD experiments carried out at 0.5 mA cm^{-2} allowed to determine a specific capacitance of 2.08 mF cm^{-2}.

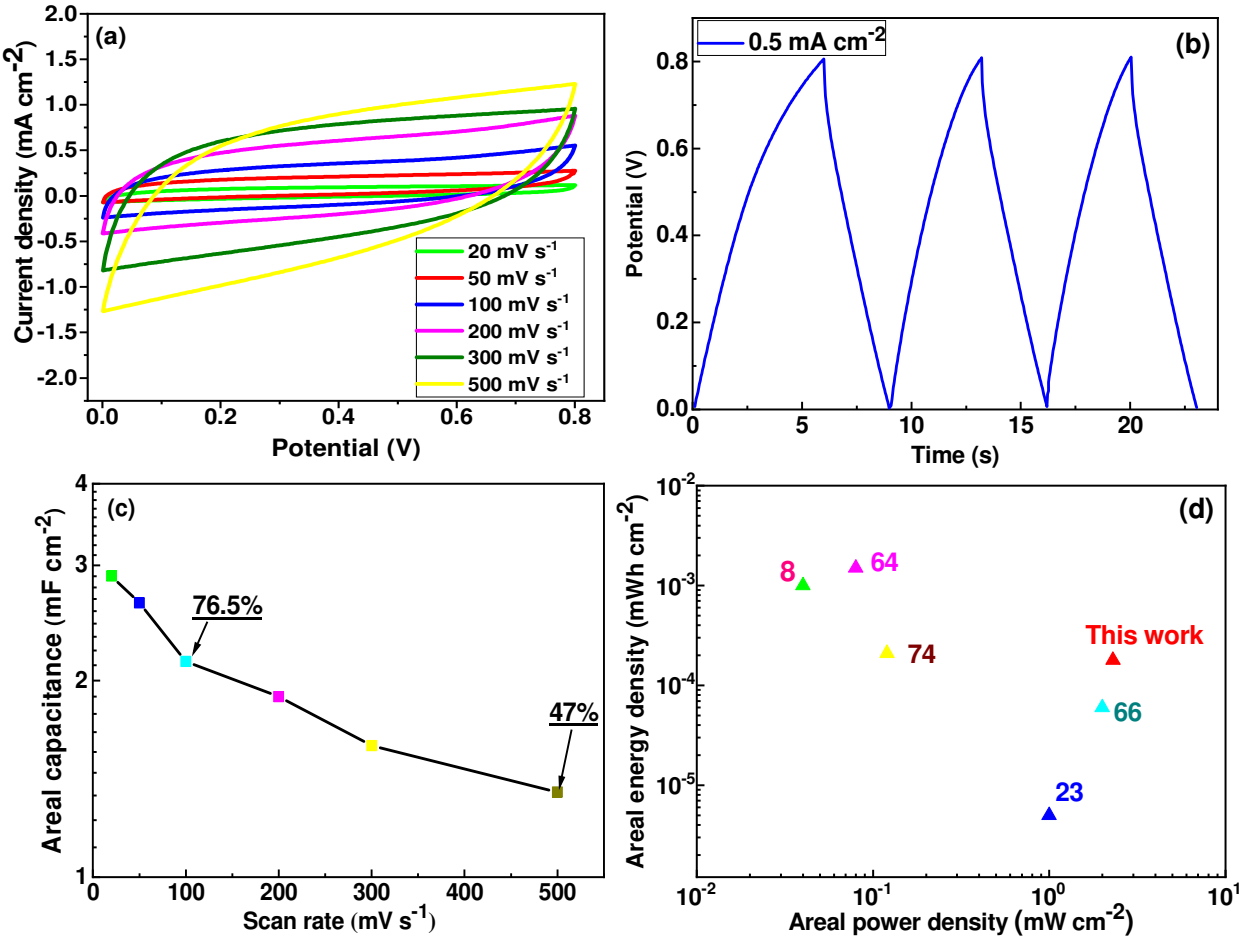

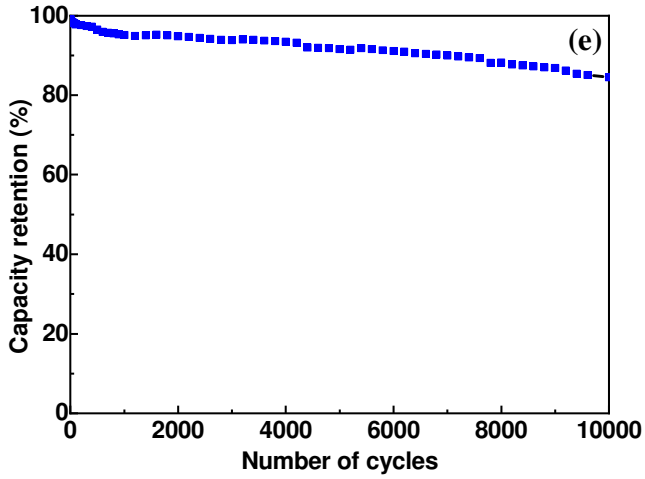

Figure 12. (a) CV curves of H–TiO_2 /SiNW symmetric electrochemical cell collected at various scan rates (potential window: -0.4 to +0.3 V), **(b)** GCD profiles of the device charged at 0.5 mA cm^{-2}, **(c)** specific capacitance *versus* scan rate, **(d)** Ragone plot, **(e)** Capacitance retention percentage of the H–TiO_2 /SiNW symmetric electrochemical ~~super~~capacitor for 10,000 cycles at 0.5 mA cm^{-2}.

The energy density was calculated from a two-electrode cell as an operating device using $E = \frac{0.5}{3.6} C(dV)^2$,where C and V correspond respectively the specific capacitance and potential window. Further, energy and power densities values of 0.179 µWhcm^{-2} and 2.13 mWcm^{-2} were determined from the GCD plots at 0.5 mAcm^{-2}, respectively.

For comparison, **Figure 12d** summarizes the literature data on cell energy density and power density. **Figure 12e** depicts the cyclability test carried out at 0.5 mA cm^{-2} up to 10,000 cycles, which showed retention of ~84.6% of the initial capacitance. Thus, the results reveal excellent capacitive feature of the H-TiO_2/SiNW in this 2-electrode device configuration.

4. Conclusion

In this paper, we compared electrochemical properties of silicon nanowires (SiNW) covered with a TiO_2 thin film. The TiO_2 layer was coated on the SiNW using atomic layer deposition (ALD), some samples of TiO_2/SiNW were subjected to a hydrogen atmosphere annealing (H-TiO_2/ SiNW) and the others in the open air (air-TiO_2/SiNW) both at 400 °C for

4 h. The effect of hydrogenation treatment on the specific capacitance of the TiO_2/SiNW electrodes was investigated. Our results revealed that hydrogenation improved substantially the energy storage ability of H-TiO_2/SiNW as electrode material for electrochemical ~~super~~capacitors. Indeed, after hydrogenation, H-TiO_2/SiNW featured a specific capacity of 3.36 mF cm^{-2} at 0.035 mA cm^{-2} in 1 M Na_2SO_4, a value 6 times larger than that recorded for air-TiO_2/SiNW electrode. The electrode maintained ~81% of its original specific capacitance after complete 30,000 cycles at 0.1 mA cm^{-2} (potential window: -0.4 – +0.3 V) in 1 M Na_2SO_4. Furthermore, H-TiO_2/SiNW//H-TiO_2/SiNW symmetric ~~super~~capacitor device was assembled and exhibited energy and power densities of about 0.179 µWh$cm^{-2}$and 2.13 mWcm^{-2}, respectively, determined from the galvanostatic charge/discharge plots at 0.5 mA cm^{-2} in 1 M Na_2SO_4 with 84.6% retention of the original capacitance value after 10,000 cycles. The capacitance improvement of H–TiO_2/SiNW can be ascribed to an increase of the density of hydroxyl groups and carrier density on TiO_2 surface. The results obtained in this work hold great promise for the application of ALD technique and hydrogenation for the design of high-performance electrode materials for energy storage.

Acknowledgements

The Centre National de la Recherche Scientifique (CNRS), the University of Lille, and the Hauts-de-France region are acknowledged for financial support. The authors also thank the Taif University Researchers Supporting Project number (TURSP-2020/03), Taif University, Taif, Saudi Arabia.

References

[1] M. Turgut Gür, Review of electrical energy storage technologies, Materials and Systems: challenges and prospects for large-scale grid storage, Energy Environ. Sci. 11 (2018) 3055-3055.

[2] Y. Wang, Y. Song, Y. Xia, Electrochemical capacitors: mechanism, material, systems, characterization and applications, Chem. Soc. Rev. 45 (2016) 5925-5950.

[3] H. Zhang, Y. Cao, M. Oliver, P. Dong, M. Ye, J. Shen, Recent advances in micro-supercapacitors, Nanoscale 11 (2019) 5807-5821.

[4] C. Lethien, J. Bideau, T. Brousse, Challenges and prospects of 3D micro-supercapacitors for powering the internet of things, Energy Environ. Sci. 12 (2019) 96-115.

[5] C. Shen, S. Xu, Y. Xie, L. Lin, A review of on-chip micro supercapacitors for integrated self-powering systems, J. Microelectromechanical Syst. 26 (2017) 949 - 965.

[6] M. Beidaghi, Y. Gogotsi, Capacitive energy storage in micro-scale devices: recent advances in design and fabrication of micro-supercapacitors, Energy Environ. Sci. 7 (2014) 867-884.

[7] A. S. Arico, P. Bruce, B. Scrosati, J.-M. Tarascon, W. V. Schalkwijk, Nanostructured materials for advanced energy conversion and storage devices, Nature Mater. 4 (2005) 366-377.

[8] R. R. Devarapalli, S. Szunerits, Y. Coffinier, M. V. Shelke, R. Boukherroub, Glucose-Derived Porous Carbon-Coated Silicon Nanowires as Efficient Electrodes for Aqueous Micro-Supercapacitors, ACS Appl. Mater. Interfaces 8 (2016) 4298−4302.

[9] F. Thissandier, P. Gentile, T. Brousse, G. Bidan, S. Sadki, Are Tomorrow's Micro-Supercapacitors Hidden in Forest of Silicon Nanotrees?, J. Power Sources 269 (2014) 740-746.

[10] D. Aradilla, P. Gentile, G. Bidan, V. Ruiz, P. Gómez-Romero, T. J. S. Schubert, H. Sahin, E. Frackowiak, S. Sadki, High Performance of Symmetric Micro-Supercapacitors Based on Silicon Nanowires UsingN-Methyl-N-propylpyrrolidiniumbis -(trifluoromethylsulfonyl)imide as Electrolyte, Nano Energy 9 (2014) 273-281.

[11] N. Berton, M. Brachet, F. Tissandier, J. Le Bideau, P. Gentile, G. Bidan, T. Brousse, S. Sadki, Wide-Voltage-Window Silicon Nanowire Electrodes for Micro-Supercapacitors via Electrochemical Surface Oxidation in IonicLiquid Electrolyte, Electrochem. Commun. 41 (2014) 31-34.

[12] L. Mai, X. Tian, X. Xu, L. Chang, L. Xu, Nanowire Electrodes for Electrochemical Energy Storage Devices, Chem. Rev. 114 (2014) 11828-11862.

[13] C. K. Chan, H. Peng, G. Liu, X. F. Zhang, R. A. Huggins, Y. Cui, High performance lithium battery anodes using silicon nanowires, Nature Nanothechnol. 3 (2008) 31-35.

[14] L. F. Cui, R. Ruffo, C. K. Chan, H. Peng, Y. Cui, Crystalline-amorphous core-shell silicon nanowires for high capacity and high current battery electrodes, Nano Lett. 9 (2009) 491-495.

[15] X. Su, Q. Wu, J. Li, X. Xiao, A. Lott, W. Lu, B. W. Sheldon, J. Wu, Silicon-based nanomaterials for lithium-ion Batteries: A review, Adv. Energy Mater. 4 (2014) 1300882.

[16] F. Lu, M. Qiu, X. Qi, L. Yang, J. Yin, G. Hao, X. Feng, J. Li, J. Zhong, Electrochemical properties of high-power supercapacitors using ordered NiO coated Si nanowire array electrodes, Appl. Phys. A 104 (2011) 545-550.

[17] D. P. Dubal, D. Aradilla, G. Bidan, P. Gentile, T. J. S. Schubert, J. Wimberg, S. Sadki, P. Gomez-Romero, 3D hierarchical assembly of ultrathin MnO2 nanoflakes on silicon nanowires for high performance micro-supercapacitors in Li- doped ionic liquid, Sci. Rep. 5 (2015) 9771.

[18] H.-C. Han, C.-W. Chong, S.-B. Wang, D. Heh, C.-A. Tseng, Y.-F. Huang, S. Chattopadhyay, K.-H. Chen, C.-F. Lin, J.-H. Lee, L.-C. Chen, High k nanophase zinc oxide on biomimetic silicon nanotip array as supercapacitors, Nano Lett. 13 (2013) 1422-1428.

[19] D. Aradilla, F. Gao, G. Lewes-Malandrakis, W. Müller-Sebert, P. Gentile, S. Pouget, C. E. Nebel, G. Bidan, Powering electrodes for high performance aqueous micro-

supercapacitors: Diamond-coated silicon nanowires operating at a wide cell voltage of 3 V, Electrochim. Acta 242 (2017) 173-179.

[20] D. Aradilla, F. Gao, G. Lewes-Malandrakis, W. Muller-Sebert, D. Gaboriau, P. Gentile, B. Iliev, T. Schuber, S. Sadki, G. Bidan, C. E. Nebel, A step forward into hierarchically nanostructured materials for high performance micro-supercapacitors: diamond coated SiNW electrodes in protic ionic liquid electrolyte, Electrochem. Commun. 63 (2016) 34-38.

[21] J. P. Alper, M. Vincent, C. Carraro, R. Maboudian, Silicon carbide coated silicon nanowires as robust electrode material for aqueous micro-supercapacitor, Appl. Phys. Lett. 100 (2012) 163901.

[22] X. Chen, S. Mao, Titanium Dioxide Nanomaterials: Synthesis, Properties, Modifications, and Applications, Chem. Rev. 107 (2007) 2891−2959.

[23] X. Lu, G. Wang, T. Zhai, M. Yu, J. Gan, Y. Tong, Y. Li, Hydrogenated TiO_2 nanotube arrays for supercapacitors, Nano Lett. 12 (2012) 1690-1696.

[24] M. Salari, K. Konstantinov, H. Liu, Enhancement of the capacitance in TiO_2 nanotubes through controlled introduction of oxygen vacancies, J. Mater. Chem. 21 (2011) 5128-5133.

[25] H. Li, Z. Chen, C. K. Tsang, Z. Li, X. Ran, C. Lee, B. Nie, L. Zheng, T. Hung, J. Lu, B. Pan, Y. Y. Li, Electrochemical doping of anatase TiO_2 in organic electrolytes for high-performance supercapacitors and photocatalysts, J. Mater. Chem. A 2 (2014) 229-236.

[26] K. Lee, A. Mazare, P. Schmuki, One-Dimensional Titanium Dioxide Nanomaterials: Nanotubes, Chem. Rev. 114 (2014) 9385−9454.

[27] V. Trifiletti, N. Manfredi, A. Listorti, D. Altamura, C. Giannini, Si. Colella, G. Gigli, A. Rizzo, Engineering TiO_2/perovskite planar heterojunction for hysteresis-less solar cells, Adv. Mater. Interfaces 3 (2016) 1600493.

[28] H. Wang, H. Li, W. Cai, P. Zhang, S. Cao, Z. Chen, Z. Zang, Challenges and strategies relating to device function layers and their integration toward high-performance inorganic perovskite solar cells, Nanoscale 12 (2020) 14369-14404

[29] F. Konstantinou, A. Shougee, T. Albrecht, K Fobelets, TiO_2 coated Si nanowire electrodes for electrochemical double layer capacitors in room temperature ionic liquid, J. Phys. D: Appl. Phys. 50 (2017) 415503.

[30] C. Zhang, S. Tian, L. Li, J. Zhou, F. Xue, C. P. Wong, Enhanced micro-supercapacitors in aqueous electrolyte based on Si nanowires coated with TiO_2, J. Mater. Sci.: Mater. Electron. 30 (2019) 8763-8770.

[31] X. Meng, X. Q. Yang, X. Sun, Emerging applications of atomic layer deposition for lithium-ion battery studies, Adv. Mater. 24 (2012) 3589-3615.

[32] E. Memarz, P. Kalisvaart, K. Cui, ALD TiO_2 coated silicon nanowires for lithium ion battery anodes with enhanced cycling stability and coulombic efficiency, Phys. Chem. Chem. Phys. 15 (2013) 13646-13657.

[33] M. Salari, S. Aboutalebi, H. K. Konstantinov, H. K. Liu, A highly ordered titania nanotube array as a supercapacitor electrode, Phys. Chem. Chem. Phys. 13 (2011) 5038–5041.

[34] M. S. Kim, T. W. Lee, J. H. Park, Controlled TiO_2 Nanotube Arrays as an Active Material for High Power Energy-Storage Devices, J. Electrochem. Soc. 156 (2009) A584–A588.

[35] J. Wang, J. L. Polleux, J. Lim, B. Dunn, Pseudocapacitive contributions to electrochemical energy storage in TiO_2 (anatase) nanoparticles, J. Phys. Chem. C 111 (2007) 14925–14931.

[36] F. Fabregat-Santiago, E. M. Barea, J. Bisquert, G. K. Mor, K. Shankar, C. A. Grimes, High carrier density and capacitance in TiO_2 nanotube arrays induced by electrochemical doping, J. Am. Chem. Soc. 130 (2008) 11312–11316.

[37] T. Xia, C. Zhang, N. A. Oyler, X. Chen, Hydrogenated TiO_2 nanocrystals: a novel microwave absorbing material, Adv. Mater. 25 (2013) 6905-6910.

[38] O. Fellahi, R. K. Sarma, M. R. Das, R. Saikia, L. Marcon, Y. Coffinier, T. Hadjersi, M. Maamache, R. Boukherroub, The antimicrobial effectof silicon nanowires decorated with silver and copper nanoparticles, Nanotechnology 24 (2013) 495101.

[39] A. Hamdi, L. Boussekey, P. Roussel, A. Addad, H. Ezzaouia, R. Boukherroub, Y. Coffinier, Hydrothermal preparation of MoS_2/TiO_2/Si nanowires composite with enhanced photocatalytic performance under visible light, Mater. Design 109 (2016) 634-643.

[40] M. Mehta, N. Kodan, S. Kumar, A. Kaushal, L. Mayrhofer, M. Walter, M. Moseler, A. Dey, S. Krishnamurthy, S. Basu, A. P. Singh, Hydrogen treated anatase TiO_2: a new experimental approach and further insights from theory, J. Mater. Chem. A 4 (2016) 2670-2681.

[41] J. Song, M. Zheng, B. Zhang, Q. Li, F. Wang, L. Ma, Y. Li, C. Zhu, L. Ma, W. Shen, Fast Growth of Highly Ordered TiO_2 Nanotube Arrays on Si Substrate under High-Field Anodization, Nano-Micro Lett. 9 (2017) 13.

[42] X. Chen, L. Liu, P.Y. Yu, S. Mao, Increasing solar absorption for photocatalysis with black hydrogenated titanium dioxide nanocrystals, Science 331 (2011) 746-750.

[43] M. S. Lazarus, T. K. Sham, X-ray photoelectron spectroscopy (XPS) studies of hydrogen reduced rutile (TiO_{2-x}) surfaces, Chem. Phys. Lett. 92 (1982) 670-673.

[44] G. Wang, H. Wang, Y. Ling, Y. Tang, X. Yang, R. C. Fitzmorris, C. Wang, J. Z. Zhang, Y. Li, Hydrogen-treated TiO_2 nanowire arrays for photo-electrochemical water splitting, Nano Lett. 11 (2011) 3026-3033.

[45] Y. Chen, Q. Tao, W. Fu, H. Yang, X. Zhou, S. Su, D. Ding, Y. Mu, X. Li, M. Li, Enhanced photoelectric performance of PbS/CdS quantum dot co-sensitized solar cells via hydrogenated TiO_2 nanorod arrays, Chem. Commun. 50 (2014) 9509-9512.

[46] P. Raghunath, W. F. Huang, M. C. Lin, Quantum chemical elucidation of the mechanism for hydrogenation of TiO_2 anatase crystals, J. Chem. Phys. 138 (2013) 154705.

[47] A. Naldoni, M. Allieta, S. Santangelo, M. Marelli, F. Fabbri, S. Cappelli, C. L. Bianchi, R. Psaro, V. Dal Santo, Effect of Nature and Location of Defects on Band gap Narrowing in Black TiO_2 Nanoparticles, J. Am. Chem. Soc. 134 (2012) 7600-7603.

[48] L. Tian, J. Xu, M. Just, M. Green, L. Liu, X. Chen, Broad range energy absorption enabled by hydrogenated TiO_2 nanosheets: from optical to infrared and microwave, J. Mater. Chem. C 5 (2017) 4645-4653.

[49] Y. Lu, W.-J. Yin, K.-L. Peng, K. Wang, Q. Hu, A. Selloni, F.-R. Chen, L.-M. Liu, M.-L. Sui, Self-hydrogenated shell promoting photocatalytic H_2 evolution on anatase TiO_2, Nature Commun. 9 (2018) 2752.

[50] J. Zhang, Y. Wang, J. Wu, X. Shu, C. Yu, J. Cui, Y. Qin, Y. Zhang, P. M. Ajayan, Y. Wu, Remarkable supercapacitive performance of TiO_2 nanotube arrays by introduction of oxygen vacancies, Chem. Eng. J. 313 (2017) 1071-1081.

[51] H. Wu, D. Li, X. Zhu, C. Yang, D. Liu, X. Chen, Y. Song, L. Lu, High-performance and renewable supercapacitors based on TiO_2 nanotube array electrodes treated by an electrochemical doping approach, Electrochim. Acta 116 (2014) 129-136.

[52] A. Soam, P. Kavle, A. Kumbhar, R. O. Dusane, Performance enhancement of micro-supercapacitor by coating of graphene on silicon nanowires at room temperature,, Curr. Appl. Phys. 17 (2017) 314-320.

[53] L. Qiao, A. Shougee, T. Albrecht, K. Fobelets, Oxide-coated silicon nanowire array capacitor electrodes in room temperature ionic liquid, Electrochim. Acta 210 (2016) 32-37.

[54] F. Gao, G. Lewes-Malandrakis, M. T. Wolfer, W. Muller-Sebert, P. Gentile, D. Aradilla, T. Schubert, C. E. Nebel, Diamond-coated silicon wires for supercapacitor applications in ionic liquids, Diamond Relat. Mater. 51 (2015) 1-6.

[55] P. Lu, P. Ohlckers, L. Müller, S. Leopold, M. Hoffmann, K. Grigoras, J. Ahopelto, M. Prunnila, X. Chen, Nano fabricated silicon nanorod array with titanium nitride coating for on-chip supercapacitors, Electrochem. Commun. 70 (2016) 51-55.

[56] S. Xiao, F. Bi, L. Zhao, L. Wang, G. Gai, Design and synthesis of H-TiO_2/MnO_2 core–shell nanotube arrays with high capacitance and cycling stability for supercapacitors, J. Mater. Sci. 52 (2017) 7744-7753.

[57] A. Balducci, D. Belanger, T. Brousse, J. W. Long, W. Sugimoto, Perspective—A guideline for reporting performance metrics with electrochemical capacitors: From electrode materials to full devices, J. Electrochem. Soc. 164 (2017) A1487.

[58] L. Y. Chen, J. L. Kang, Y. Hou, P. Liu, T. Fujita, A. Hirata, M. W. Chen, High-energy-density nonaqueous MnO_2@nanoporous gold based supercapacitors, J. Mater. Chem. A 1 (2013) 9202-9207.